Synthesis, Crystal and Electronic Structures of the Titanium-rich Bismuthides AE3Ti8Bi10 (AE = Sr, Ba, Eu)

Journal:	*Inorganic Chemistry*
Manuscript ID	ic-2018-01952a.R2
Manuscript Type:	Article
Date Submitted by the Author:	n/a
Complete List of Authors:	Ovchinnikov, Alexander; University of Delaware, Chemistry and Biochemistry Bobev, Svilen; University of Delaware, Chemistry and Biochemistry

Synthesis, Crystal and Electronic Structures of the Titanium-rich Bismuthides $AE_3Ti_8Bi_{10}$ (AE = Sr, Ba, Eu)

Alexander Ovchinnikov and Svilen Bobev*

Department of Chemistry and Biochemistry, University of Delaware, Newark, Delaware 19716, United States

KEYWORDS bismuthides, crystal structure, electronic structure, metal-metal bonding, titanium

Supporting Information Placeholder

ABSTRACT: Three isotypic compounds with the chemical formula $AE_3Ti_8Bi_{10}$ (AE = Sr, Ba, Eu) have been obtained via both high-temperature solid state and flux growth reactions. Their crystal structure, representing a new type (space group $P6_3/mmc$, Pearson symbol $hP42$), features an open framework composed of interlinked $TiBi_5$ square pyramids and $TiBi_6$ octahedra. The Ti–Bi substructure is penetrated by infinite columns of face-sharing AE_6 polyhedra centered by Bi atoms. First-principle calculations and physical property measurements indicate metallic behavior and absence of localized magnetic moments on the Ti atoms. Analysis of the chemical bonding reveals strong Ti–Bi and Ti–Ti bonds. The latter demonstrate classic two-center, as well as multicenter interactions.

INTRODUCTION

Solid compounds of transition metals (TM) with the group 15 elements (pnictogens, *Pn*) represent a vast class of materials, commonly referred to as pnictides. They adopt a plethora of crystal structure types and display a wide variety of physical properties. The large diversity of experimentally observed atomic arrangements results from different kinds of chemical bonding: covalent interactions between the TM and *Pn* atoms, formation of oligomeric or polymeric *Pn* units, metal–metal bonding, and electron transfer onto the anionic substructure from electropositive metals, such as alkali, alkaline-earth, or rare-earth metals, in multinary compounds with partially ionic bonding.

Combinations of distinct chemical bonding not only provide conditions for realization of varying crystal structures but can also engender notable structural complexity.[1–6] The interplay of chemical composition and peculiar bonding frequently gives rise to interesting properties in transition metal pnictides. Some of these compounds have been proposed as potential thermoelectric materials owing to their appropriate electronic properties, coupled with low thermal conductivity, e.g., $Yb_{14}MnSb_{11}$[7] or ATM_4Pn_{12}, where A is an alkali, alkaline-earth, or rare-earth metal.[8] The binary manganese bismuthide MnBi has been studied as a promising permanent magnet.[9] More recently, the discovery of superconductivity in iron arsenides hallmarked a whole new era in pnictide research.[10]

Despite the considerable advances in pnictide chemistry of late transition metals, the field of early transition metal pnictides remains scarcely explored, especially when multinary compounds are concerned. Compositions bearing electropositive metals A, e.g. alkali, alkaline-earth or rare-earth metals, are of particular interest since they often show an amalgamation of metal and salt-like features, due to the significant polarization of the A–Pn bonds. Remarkable structural complexity is observed in the alkali metal–Nb–As systems, boasting As_n olygomers and mixed-valent Nb species.[11,12] Considering the heavier pnictogens Sb and Bi, a number of crystalline phases showing complex combinations of extended Ti–Ti and Pn–Pn bonding are known in the AE–Ti–Pn and RE–Ti–Pn systems, where AE and RE stand for alkaline-earth and rare-earth metal, respectively.[13–16] Interestingly, despite a high chemical affinity of Ti to Bi, reflected in high mutual solubility in the liquid state and the formation of several binary phases, structurally characterized multinary titanium bismuthides in the discussed systems are limited to the Heusler-type $Li_{3-x}Ti_xBi$,[17] La_3TiBi_5,[18,19] displaying one dimensional linear Bi chains and face-sharing $TiBi_6$ columns, and $AE_5Ti_{12}Bi_{19+x}$ (AE = Sr, Ba, Sr+Eu) with a complex three-dimensional Ti–Bi substructure.[20]

In this contribution, we present a new family of ternary titanium bismuthides $AE_3Ti_8Bi_{10}$ (AE = Sr, Ba, Eu). These compounds crystallize in their own structure type and show an intricate chemical bonding pattern.

EXPERIMENTAL DETAILS

Synthesis. All manipulations were performed in an argon-filled glovebox. Polycrystalline samples of $AE_3Ti_8Bi_{10}$ (AE = Sr, Eu) were prepared by direct combination of the elements in Nb tubes, weld-shut under

high-purity argon. Stoichiometric mixtures of *AE*, Ti, and Bi (Alfa Aesar, all with purity >99.9 wt. % metal basis) were heated up to 923 K with 200 K/h, held at this temperature for 48 h and cooled down to room temperature with 50 K/h. After that, the obtained product was ground, pelletized, and subjected to a second annealing with the same temperature profile. $Ba_3Ti_8Bi_{10}$ could not be prepared from the elements at any temperature between 773 K and 1023 K, but it was produced in single-crystalline form by the metal flux method described next.

Single crystals of $AE_3Ti_8Bi_{10}$ (*AE* = Sr, Ba, Eu) were grown from liquid lead. For *AE* = Sr, Eu, mixtures of the elements with the ratio *AE* : Ti : Bi : Pb = 3 : 8 : 10 : 50 were loaded in alumina crucibles topped with quartz wool and sealed in evacuated fused silica tubes. The tubes were heated to 1273 K with 200 K/h, kept at this temperature for 24 h and cooled down to 823 K with 2 K/h. At this temperature, the ampules were taken out of the furnace and the liquid Pb flux was removed by centrifugation. The quartz tubes were crack-opened in the glovebox and the crystals of $AE_3Ti_8Bi_{10}$ (*AE* = Sr, Eu), having predominantly rod-like morphology, were mechanically extracted from the crucibles. The Eu sample contained a small amount of $EuBi_3$, crystallized as intergrown cubes. The crystalline rods of $AE_3Ti_8Bi_{10}$ were up to 0.3 mm in width and 2 mm in length. In the case of Ba, the above-described procedure resulted in $Ba_5Ti_{12}Bi_{19+x}$[20] as the major phase. With an optimized synthetic protocol, sub-millimeter-sized single crystals of $Ba_3Ti_8Bi_{10}$ were grown from the initial composition Ba : Ti : Bi : Pb = 3 : 8 : 10 : 160. The mixture was heated up to 973 K with 200 K/h, annealed at this temperature for 30 h and cooled down to 823 K with 5 K/h, where the Pb flux was centrifuged out.

Powder X-ray diffraction (PXRD). PXRD patterns of the prepared samples were recorded in reflection mode on a Rigaku Miniflex diffractometer (Cu K_α radiation, λ = 1.5418 Å) operating inside a nitrogen-filled glovebox to prevent deterioration of the samples in ambient atmosphere. Data were collected between 5° and 75° with a step size of 0.05° and 2 s/step counting time. Qualitative Rietveld refinements were performed using the JANA2006 software.[21]

Single-crystal X-ray diffraction (SCXRD). Suitable single crystals of $AE_3Ti_8Bi_{10}$ were cut under dry Paratone N oil and mounted on low-background plastic loops. To prevent degradation of the samples, the loops were placed in a cold nitrogen stream at 200 K, which froze the oil with the embedded crystal. Data collection was done on a Bruker APEX DUO CCD diffractometer equipped with monochromated Mo K_α radiation (λ = 0.71073 Å). The raw data were integrated using the SAINT software.[22] Semiempirical absorption correction was introduced using SADABS.[23] Crystal structures were solved by direct methods and refined by full matrix least-squares methods on F^2 using SHELXL.[24] Atomic coordinates were standardized using STRUCTURE TIDY.[25] Details of the data collection, and selected crystallographic parameters are summarized in Tables 1 and 2.

Table 1. Data collection details and selected crystallographic data for $AE_3Ti_8Bi_{10}$ (*AE* = Sr, Ba, Eu; space group $P6_3/mmc$, Z = 2, T = 200 K, Mo K_α λ = 0.71073 Å)

Chemical formula	$Sr_3Ti_8Bi_{10}$	$Ba_3Ti_8Bi_{10}$	$Eu_3Ti_8Bi_{10}$
fw/ g mol^{-1}	2735.86	2885.02	2928.88
a/ Å	10.986(2)	11.108(2)	10.966(1)
c/ Å	10.183(2)	10.285(2)	10.136(1)
V/ Å^3	1064.3(4)	1099.1(5)	1055.5(3)
ρ_{calc}/ g cm^{-3}	8.54	8.72	9.22
$\mu_{MoK\alpha}$/ cm^{-1}	925.4	876.8	945.7
R_1 [$I > 2\sigma(I)$][a]	0.035	0.024	0.030
wR_2 [$I > 2\sigma(I)$][a]	0.071	0.051	0.059
R_1 [all data][a]	0.051	0.031	0.041
wR_2 [all data][a]	0.077	0.053	0.064
$\rho_{max,min}$/ e Å^{-3}	2.09, –2.41	1.53, –1.27	1.95, –1.88

[a] $R_1=\sum||F_o|-|F_c||/\sum|F_o|$; $wR_2=[\sum[w(F_o^2-F_c^2)^2]/\sum[w(F_o^2)^2]]^{1/2}$, where $w = 1/[\sigma^2F_o^2+(AP)^2+(BP)]$, and $P = (F_o^2+2F_c^2)/3$; *A*, *B* are the respective weight coefficients (see CIF in the supporting information). CIFs have also been deposited with reference CSD numbers 1855587–89.

First-principle calculations. Electronic structure calculations were performed for $Sr_3Ti_8Bi_{10}$ and $Ba_3Ti_8Bi_{10}$ within the density functional theory framework using the TB-LMTO-ASA code.[26] The Von Barth-Hedin implementation of the local density approximation (LDA) functional was employed[27] and the Brillouin zone was sampled by a 16×16×16 *k*-point grid after checking for convergence. To satisfy the atomic sphere approximation (ASA), an introduction of empty spheres was necessary. Chemical bonding was studied using the Crystal Orbital Hamilton Population analysis (COHP) and Electron Localization Function (ELF), as implemented in TB-LMTO-ASA. For the Bi–Bi contacts in the structure, the two shortest symmetrically independent distances were analyzed.

Physical property measurements. Four-contact electrical resistivity measurements were done for the $Sr_3Ti_8Bi_{10}$ and $Eu_3Ti_8Bi_{10}$ samples on a Quantum Design Physical Property Measurement System (PPMS) in the temperature range 3–300 K. Metal wires were attached to rod-like single crystals with a length of approximately 1.5–2.0 mm using a conductive silver paint. Temperature dependence of the magnetization was measured for the $AE_3Ti_8Bi_{10}$ samples (*AE* = Sr, Ba, Eu) on the PPMS in

the temperature range 3–300 K under external fields between 20 Oe and 70 kOe. The measured samples, consisting of several randomly oriented single crystals, were enclosed in low-background gel-cap holders stuffed with quartz wool. For comparison, similar magnetic measurements were conducted on sintered pellets of $AE_3Ti_8Bi_{10}$ (AE = Sr, Eu), yielding results consistent with the hand-picked crystals. A Honda-Owen correction was applied to the data to take possible ferromagnetic contributions into account.[28,29]

Table 2. Atomic coordinates and equivalent displacement parameters (Å^2) for $AE_3Ti_8Bi_{10}$

Atom	Site	x	y	z	U_{eq}[a]
		$Sr_3Ti_8Bi_{10}$			
Sr	6*h*	0.1276(1)	2*x*	1/4	0.023(1)
Ti1	6*h*	0.5818(2)	2*x*	1/4	0.016(1)
Ti2	6*g*	1/2	0	0	0.015(1)
Ti3	4*f*	1/3	2/3	0.0285(5)	0.018(1)
Bi1	12*k*	0.19335(3)	2*x*	0.57097(5)	0.017(1)
Bi2	6*h*	0.43588(5)	2*x*	1/4	0.016(1)
Bi3	2*a*	0	0	0	0.023(1)
		$Ba_3Ti_8Bi_{10}$			
Ba	6*h*	0.12725(6)	2*x*	1/4	0.020(1)
Ti1	6*h*	0.5824(2)	2*x*	1/4	0.017(1)
Ti2	6*g*	1/2	0	0	0.017(1)
Ti3	4*f*	1/3	2/3	0.0340(4)	0.018(1)
Bi1	12*k*	0.19622(2)	2*x*	0.57144(5)	0.017(1)
Bi2	6*h*	0.43709(3)	2*x*	1/4	0.017(1)
Bi3	2*a*	0	0	0	0.021(1)
		$Eu_3Ti_8Bi_{10}$			
Eu	6*h*	0.12788(6)	2*x*	1/4	0.024(1)
Ti1	6*h*	0.5826(2)	2*x*	1/4	0.012(1)
Ti2	6*g*	1/2	0	0	0.017(1)
Ti3	4*f*	1/3	2/3	0.0281(4)	0.018(1)
Bi1	12*k*	0.19219(3)	2*x*	0.57042(5)	0.017(1)
Bi2	6*h*	0.43647(4)	2*x*	1/4	0.017(1)
Bi3	2*a*	0	0	0	0.021(1)

[a] U_{eq} is defined as one third of the trace of the orthogonalized U_{ij} tensor

Thermal analysis. Simultaneous thermo-gravimetric differential scanning calorimetry measurements (TG/DSC) were conducted on a SDT Q600 analyzer, supplied by TA Instruments. The samples were loaded in capped alumina pans. After equilibration at 323 K, the temperature was raised to 1273 K with 10 K/min. The samples were kept at this point for 1 min and then cooled down to 373 K with 10 K/min. To prevent oxidation, the measurements were done under a constant flow (100 mL/min) of high-purity argon.

RESULTS AND DISCUSSION

Synthesis. Upon systematic exploratory work of the AE–Ti–Bi ternary systems, a new compound, $Eu_3Ti_8Bi_{10}$ was serendipitously discovered from an experiment aimed at the preparation of the hitherto unknown $Eu_5Ti_{12}Bi_{19+x}$.[20] Direct synthesis of $Eu_3Ti_8Bi_{10}$ from the elements produced an almost phase-pure material according to PXRD (Figure S1). A small amount of a $EuBi_3$ impurity[30] was detected in the sample. Variation of the annealing temperature or longer annealing times led to an increase in the impurity content. The best polycrystalline sample was produced after annealing the reaction mixture at 923 K for 96 h with an intermediate regrinding. Using the same synthetic procedure, we were able to obtain a powder sample of $Sr_3Ti_8Bi_{10}$. The latter always contained small amounts of the cubic $Sr_5Ti_{12}Bi_{19+x}$ phase,[20] which could not be completely eliminated by changing the synthetic conditions (Figure S1). In contrast to the Sr and Eu phases, $Ba_3Ti_8Bi_{10}$ did not form under these reactions. The major product of the reactions carried out in the temperature range 773–1023 K was the cubic $Ba_5Ti_{12}Bi_{19+x}$.[20]

Our previous experience indicates that liquid bismuth appears to be in equilibrium with the cubic $AE_5Ti_{12}Bi_{19+x}$ (AE = Sr, Ba) and with the orthorhombic $EuTi_3Bi_4$ phases in a wide temperature and compositional range.[20] Hence, single crystals of the ternary $AE_3Ti_8Bi_{10}$ compounds could not be grown from a bismuth flux. We used molten lead instead, which allowed the growth of reasonably large $AE_3Ti_8Bi_{10}$ single crystals that were suitable for transport measurements in the case of AE = Sr and Eu, by cooling down the reaction mixture from 1273 K to 823 K with 2 K/h. Increasing the amount of the AE metal in the starting mixture in comparison with the composition given in the Experimental section had a positive effect on the crystal size but resulted in the simultaneous formation of the binary phases $Sr_{11}Bi_{10}$[31] and $EuBi_3$,[30] respectively. The latter impurity was also observed in the Eu samples with the stoichiometric Eu : Ti : Bi ratio. $EuBi_3$ can be completely eliminated if the annealing temperature is lowered to 973 K, albeit at the cost of the $Eu_3Ti_8Bi_{10}$ crystal size. The almost perfectly cubic $EuBi_3$ single crystals can be easily distinguished from the rod-like $Eu_3Ti_8Bi_{10}$ crystals. In the samples with an excess of Ti, a formation of the plumbide Ti_6Pb_{5-x} was observed.[32] The Ba representative $Ba_3Ti_8Bi_{10}$ could only be prepared in high yields from a lead flux when the annealing temperature was not higher than 973 K and the cooling rate was 5 K/h. Increasing the temperature or decreasing the cooling rate always produced $Ba_5Ti_{12}Bi_{19+x}$ as the main phase.

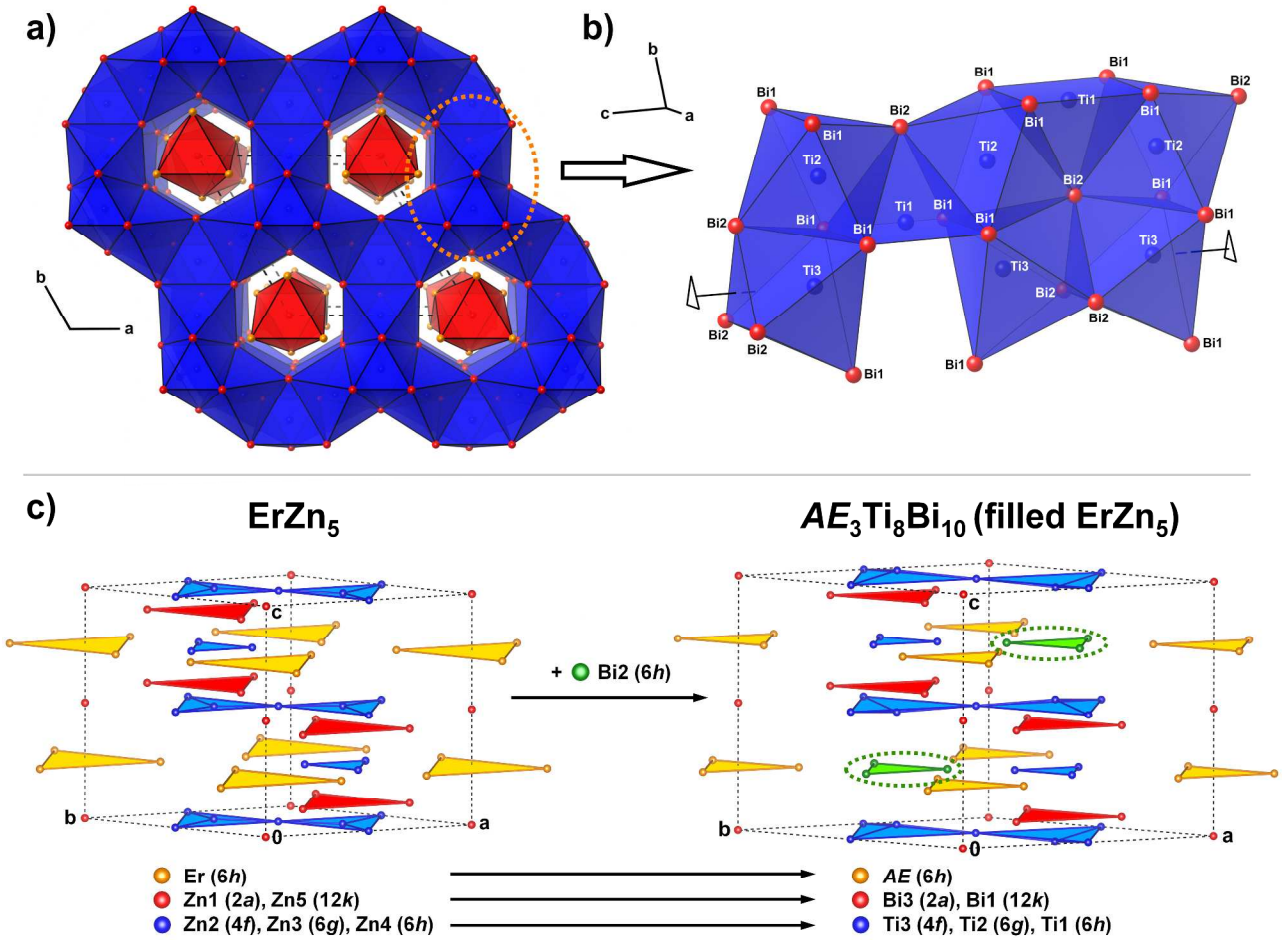

Figure 1. (a) Crystal structure of $AE_3Ti_8Bi_{10}$ (AE = Sr, Ba, Eu) drawn along [001]. (b) Part of the Ti–Bi framework showing the polyhedra interconnections. A three-fold rotation axis is indicated. (c) Crystallographic relationship between the $ErZn_5$ and $AE_3Ti_8Bi_{10}$ crystal structures.

Our TG/DSC measurements performed on the single crystals of $AE_3Ti_8Bi_{10}$ (AE = Sr, Ba, Eu) did not indicate any intrinsic thermal events up to 1273 K (Figure S2), suggesting that the samples are thermally stable in this temperature range. However, given the fact that $Ba_3Ti_8Bi_{10}$ could not be prepared from the elements and that the powder samples of $AE_3Ti_8Bi_{10}$ (AE = Sr, Eu) were always contaminated by competing compounds, it is likely that $AE_3Ti_8Bi_{10}$ (AE = Sr, Ba, Eu) are not thermodynamically stable phases, but rather kinetically arrested at the synthetic conditions.

Crystal structure. The $AE_3Ti_8Bi_{10}$ phases (AE = Sr, Ba, Eu) crystallize isostructurally in the hexagonal space group $P6_3/mmc$ (No. 194) with two formula units per unit cell. The structure constitutes a new structure type with Pearson symbol $hP42$. Titanium atoms in the crystal structure are five-fold and six-fold coordinated by Bi atoms forming a three-dimensional framework of fused $TiBi_5$ square pyramids and $TiBi_6$ octahedra. This framework contains large, one-dimensional channels running along the crystallographic c direction. These channels, in turn, accommodate infinite columns of face-shared AE_6 polyhedra which are Bi-centered (Figure 1a). The connectivity mode of the $TiBi_x$ polyhedra is rather complex and boasts varying linkage fashions (Figure 1b). The $Ti1Bi_5$ square pyramids are interconnected by common edges and share vertices and faces with the $Ti2Bi_6$ octahedra. The $Ti3Bi_6$ octahedra are linked to the $Ti1Bi_5$ pyramids through common vertices and edges. The $Ti2Bi_6$ and $Ti3Bi_6$ octahedra connect to the adjacent identical octahedra exclusively by corner- and face-sharing, respectively, whereas their interconnection is realized by face-sharing. Both symmetrically independent Bi atoms residing within the Ti–Bi framework, Bi1 and Bi2, are bonded to five adjacent Ti atoms. Altogether, taking into account the described linking patterns, the comprehensive formula of the discussed compounds can be given as $(AE_{6/2}Bi)[TiBi_{5/5}]_3[TiBi_{6/5}]_3\,[TiBi_{6/5}]_2$ (AE = Sr, Ba, Eu).

The Ti–Bi distances in $AE_3Ti_8Bi_{10}$ range between 2.78 Å and 3.05 Å (Table 3), which is in good agreement with typical bond lengths in other titanium bismuthides.[19,20,33,34] The Ti–Ti interatomic separations extend from 2.77 Å to 3.34 Å. Although, the longer side of

this distribution lies beyond the bond lengths in elemental Ti, these distances are within the range of bonding contacts in other Ti-rich intermetallic compounds.[35] The emergence of metal-metal bonding is also evidenced by our first-principle calculations (*vide infra*).

Table 3. Selected interatomic distances (Å) in $AE_3Ti_8Bi_{10}$ (AE = Sr, Ba, Eu)

Atom Pairs		AE = Sr	AE = Ba	AE = Eu
AE	—Bi2 × 2	3.391(2)	3.4338(9)	3.379(1)
	—Bi1 × 2	3.500(1)	3.5625(9)	3.4698(8)
	—Bi3 × 2	3.517(2)	3.5505(8)	3.5100(8)
	—Bi1 × 4	3.7176(8)	3.7917(8)	3.6974(6)
Ti1	—Bi2	2.776(5)	2.795(3)	2.775(3)
	—Bi1 × 4	2.9539(7)	2.9469(7)	2.9612(6)
	—Ti1 × 2	2.797(8)	2.809(5)	2.767(6)
	—Ti2 × 2	2.984(2)	3.020(2)	2.980(2)
	—Ti3 × 2	3.264(5)	3.341(4)	3.240(4)
Ti2	—Bi2 × 2	2.8230(6)	2.8420(6)	2.8066(4)
	—Bi1 × 4	3.0377(5)	3.0533(5)	3.0381(4)
	—Ti1 × 2	2.984(2)	3.020(2)	2.980(2)
	—Ti3 × 2	3.1847(5)	3.2257(4)	3.1783(4)
Ti3	—Bi1 × 3	2.850(2)	2.852(2)	2.861(2)
	—Bi2 × 3	2.982(4)	2.987(3)	2.982(3)
	—Ti2 × 3	3.1847(5)	3.2257(4)	3.1783(4)
	—Ti1 × 3	3.264(5)	3.341(4)	3.240(4)
Bi2	—Bi2 × 2	3.380(2)	3.458(1)	3.393(1)

The shortest Bi–Bi contact is observed for the regular triangle of Bi2 atoms on the $Ti3Bi_6$ octahedron face. The corresponding distance ranges from 3.38 Å to 3.46 Å on going from $Sr_3Ti_8Bi_{10}$ to $Ba_3Ti_8Bi_{10}$, respectively, which is far above the contacts between single-bonded Bi atoms (the Pauling radius r_{Bi} = 1.52 Å[36]). Nevertheless, similarly long Bi–Bi bonds are found in hypervalent anionic species, e.g. in the linear $[Bi_3]^{7-}$ moieties in $AE_{14}MgBi_{11}$ and $AE_{14}MnBi_{11}$ (AE = Ca, Sr, Ba, Eu, Yb)[37–42] and $Ba_2Mn_{1-x}Bi_2$.[6] In pnictides, hypervalent interactions are realized as a result of chemical bonding optimization in electron-rich polyanionic subunits, such as olygomers,[37–41,43] chains,[13,19,43–45] or planes.[43,46–48] After the Bi2–Bi2 contacts, the shortest distance between the Bi atoms in $AE_3Ti_8Bi_{10}$ is the Bi1–Bi1 pair between the corners of the adjacent $Ti1Bi_6$ octahedra along the c direction. This distance, however, exceeds 3.60 Å for all representatives and, as indicated by the chemical bonding analysis (*vide infra*), displays a negligible bonding interaction.

The crystal structure of $AE_3Ti_8Bi_{10}$ (AE = Sr, Ba, Eu) can be also viewed as a stuffed derivative of the $ErZn_5$ type (Figure 1c). The atomic positions in the latter follows the Wyckoff sequence *kh2gfa*. By replacing the Er atoms by AE (AE = Sr, Ba, Eu) and "coloring" the Zn substructure according to the scheme in Figure 1c, the composition of the unit cell transforms from Er_6Zn_{30} (= $ErZn_5$) to $AE_6Ti_{16}Bi_{14}$. The overall crystal structure is completed upon insertion of additional Bi atoms in position 6*h*, yielding the final composition $AE_6Ti_{16}Bi_{20}$ (= $AE_3Ti_8Bi_{10}$). Since such insertion leads to an expansion of the unit cell in the *ab* plane, the *c*/*a* ratio for $AE_3Ti_8Bi_{10}$ drops down to 0.92–0.93 in comparison with $ErZn_5$-type compounds, exhibiting *c*/*a* values of 1.03–1.04.[49]

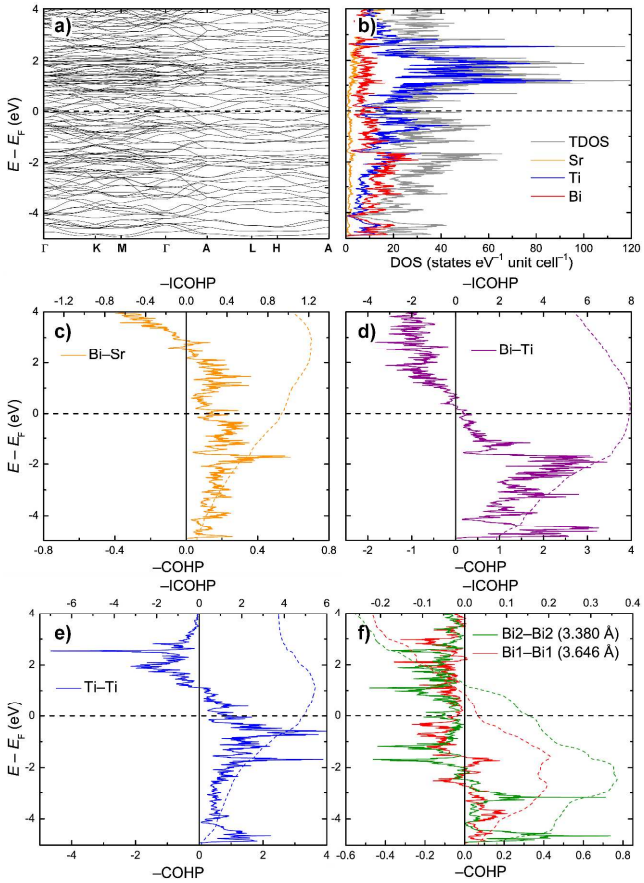

Figure 2. Electronic structure and chemical bonding in $Sr_3Ti_8Bi_{10}$. (a) Band structure along selected directions. (b) Total and projected densities of states. (c)–(f) COHP curves for selected interatomic contacts.

Electronic structure and chemical bonding. The electronic band structure and density of states (DOS) for $Sr_3Ti_8Bi_{10}$ are shown in Figure 2a and b, respectively. The manifold of electronic bands crossing the Fermi level (E_F) results in a considerable density of states at

E_F. The dispersion of the bands along the high-symmetry directions of the Brillouin zone indicates an essentially three-dimensional metallic behavior. Similar picture is observed for the Ba counterpart (Figure S3). Spin-polarized calculations converged to zero magnetic moments on the Ti atoms.

Crystal Orbital Hamilton Population analysis (COHP) reveals that the Bi–Sr, Bi–Ti and Ti–Ti contacts show bonding interactions below the Fermi level (Figure 2c, d, e). The negative integrated COHP (–ICOHP) values for the symmetrically independent Bi–Sr pairs range from 0.15 to 0.39 eV/bond. The corresponding interactions are underoptimized at E_F since unpopulated bonding states are available above the Fermi level up to $E - E_F$ = 3.0 eV. In contrast, the Bi–Ti bonds are fully optimized. The majority of the bonding states for these contacts are located below $E - E_F$ = –1.0 eV, where the strong Ti(3d)–Bi(6p) hybridization occurs. These interactions provide the main contribution to the structural stability with the individual –ICOHP addends of 1.07–1.67 eV/bond. Similarly high –ICOHP values of 0.82–1.95 eV/bond are calculated for the Ti–Ti contacts, which remain faintly underoptimized at E_F. As it is evident from the COHP curve, the Ti–Ti bonding interactions are responsible for the high DOS peaks of Ti(3d) character in the close vicinity of the Fermi level.

Unlike the above-mentioned atomic pairs, the two shortest Bi–Bi contacts in the structure show a combination of bonding and antibonding states below the Fermi level (Figure 2f). The overall interaction results in a bonding situation at E_F in both cases with the –ICOHP values of 0.15 and 0.03 eV/bond for the Bi2–Bi2 and Bi1–Bi1 contacts, respectively. Whereas the latter value is negligible, the former number is close to the corresponding measure for some of the Bi–Sr bonds. As was discussed above, the Bi2–Bi2 distance falls in the range typical for hypervalent Bi–Bi bonds. Indeed, the sharp peaks of low-lying bonding states and antibonding states located just under the Fermi level, as observed for the Bi2–Bi2 pair, appear to be a hallmark of electron-rich (hypervalent) bonds in polyanionic structures.[19,43,50]

Since the Ti–Ti interactions have the strongest effect on the total DOS at the Fermi level, it is worthy to discuss the chemical bonding within the Ti framework in more detail. The pattern of interconnected Ti atoms is shown in Figure 3a. The repeating fragment of the Ti substructure is a trigonal bipyramid $Ti1_3Ti3_2$ with all six lateral edges capped by Ti2 atoms. Alternatively, this moiety can be viewed as two interpenetrating $Ti3Ti2_3$ tetrahedra pointing in opposite directions and intersecting along the $Ti1_3$ triangle. These building blocks are interconnected by corner-sharing via Ti2 atoms. Visualization of the electron localization function (ELF) reveals a localized domain inside the principal building block in the center of the triangular base (Figure 3b). This feature points toward multicenter bonding involving the three Ti1 atoms and the two Ti3 atoms as can be seen from the section of the ELF (Figure 3c). The latter picture demonstrates flattening of the ELF around Ti3 atoms in the direction of the triangular base, which is a sign of chemical bonding interactions.[51] The Ti1–Ti2 and Ti3–Ti2 bonds appear to be two-center as indicated by ELF maxima on the lines connecting these atoms and the corresponding deformation of the ELF distribution.

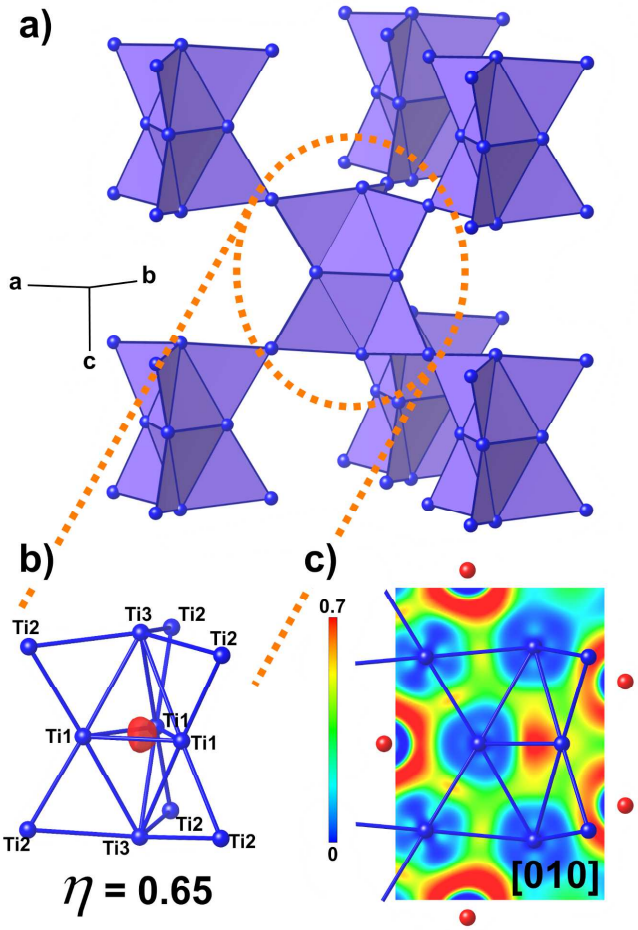

Figure 3. (a) Ti substructure in $AE_3Ti_8Bi_{10}$. (b) ELF isosurface (η = 0.65) inside the Ti skeleton in $Sr_3Ti_8Bi_{10}$. (c) ELF section through the repeating building block of the Ti framework in $Sr_3Ti_8Bi_{10}$.

Physical properties. Electrical resistivity measurements on the $AE_3Ti_8Bi_{10}$ (AE = Sr, Eu) single crystals revealed metallic behavior (Figure 4 top). The resistivity of the Eu representative was found to be approximately three times higher than that of the Sr compound, likely due to additional magnetic scattering. Below ≈ 7.5 K, a superconducting transition of the remaining Pb flux is observed. Although Pb could not be completely removed from the crystal surface, its contribution to the electrical resistivity above T_c is negligible as can be judged from the absolute values of $\rho(T)$. Magnetization measure-

ments on a sintered $Sr_3Ti_8Bi_{10}$ pellet in external fields as low as 20 Oe did not indicate any intrinsic superconducting transitions down to 3 K.

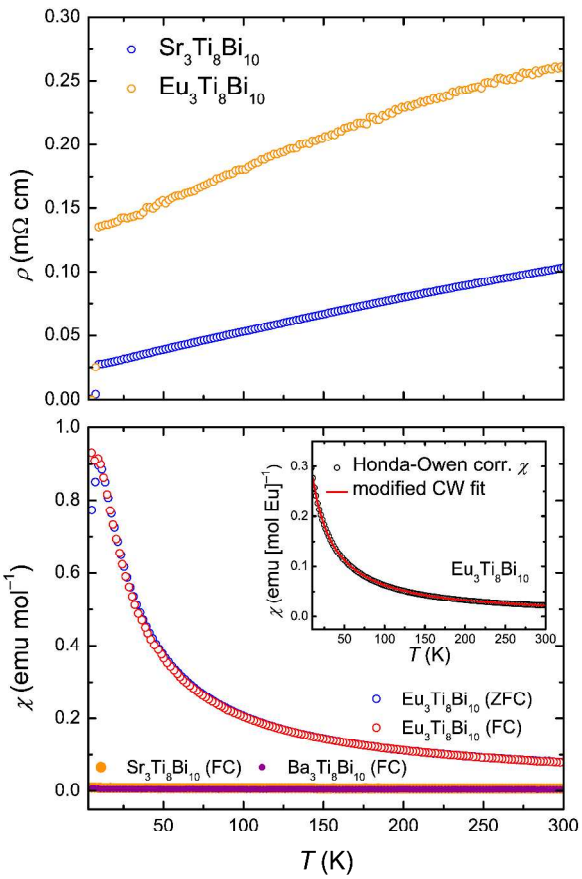

Figure 4. (top) Temperature dependence of electrical resistivity for $AE_3Ti_8Bi_{10}$ (AE = Sr, Eu). (bottom) Temperature dependence of magnetic susceptibility (H = 5 kOe) for $AE_3Ti_8Bi_{10}$ (AE = Sr, Ba, Eu). Inset: Honda-Owen corrected magnetic susceptibility for $Eu_3Ti_8Bi_{10}$ (circles) with a modified Curie-Weiss fit (red line).

Temperature dependence of the magnetic susceptibility for $AE_3Ti_8Bi_{10}$ (AE = Sr, Ba, Eu) is shown in Figure 4 bottom. In accordance with our first-principle calculations, the Ti atoms in $AE_3Ti_8Bi_{10}$ do not carry localized magnetic moments. Measurements on $Sr_3Ti_8Bi_{10}$ and $Ba_3Ti_8Bi_{10}$ revealed an almost temperature-independent paramagnetic response on the order of 10^{-3} emu/mol, indicating the prevalence of the Pauli paramagnetic contribution.

$Eu_3Ti_8Bi_{10}$ displays localized paramagnetic behavior at high temperatures. A fit of the magnetic susceptibility curve with a modified Curie-Weiss expression yields the effective magnetic moment of 7.82 μ_B, close to the theoretical value of 7.94 μ_B for free-ion Eu^{2+} ($4f^7$), and the Weiss constant $\Theta = -16.8$ K. The negative value points toward antiferromagnetic leading exchange interaction. At around 8.5 K, an antiferromagnetic transition occurs. It is worthwhile to note that this ordering temperature is close to the Néel temperature of the binary $EuBi_3$ (T_N = 7.5),[30] which was occasionally found as an impurity in our samples. However, a PXRD analysis of the ground $Eu_3Ti_8Bi_{10}$ crystals used for the measurements did not indicate any presence of $EuBi_3$, which suggests that the discussed transition is likely intrinsic.

CONCLUSIONS

A novel family of ternary titanium bismuthides, $AE_3Ti_8Bi_{10}$ (AE = Sr, Ba, Eu), has been discovered and characterized. The crystal structure of these compounds can be described as an open framework of fused $TiBi_5$ square pyramids and $TiBi_6$ octahedra. Face-sharing Bi-centered $BiAE_6$ distorted octahedra occupy channels in the Ti–Bi substructure forming infinite one-dimensional columns. Whereas the main structure-stabilizing factor is the covalent bonding between the Ti and Bi atoms, another considerable contribution stems from Ti–Ti interactions of two-center and multicenter character. The strong hybridization of the Ti(3d) states leads to a sizeable electronic DOS at the Fermi level. However, no associated electronic or magnetic instabilities are observed in the physical property data down to 3 K. The $AE_3Ti_8Bi_{10}$ samples display metallic conductivity and no local magnetic moments on the Ti atoms in the whole measured temperature range. $Eu_3Ti_8Bi_{10}$ demonstrates Curie-Weiss-type paramagnetic behavior consistent with Eu^{2+} ($4f^7$) and a sign of antiferromagnetic ordering of the Eu^{2+} moments below 8.5 K. In summary, the presented compounds provide an evidence of rich and yet scarcely explored structural chemistry in pnictides of early transition elements. More detailed analysis of the phase field may uncover new compounds with possibly interesting physical properties.

ASSOCIATED CONTENT

Supporting Information. Powder X-ray diffraction patterns for the $AE_3Ti_8Bi_{10}$ sintered pellets (AE = Sr, Eu), TG/DSC data, electronic structure calculations for $Ba_3Ti_8Bi_{10}$. This material (all supplied in PDF), as well as the crystallographic information files (CIF) are available free of charge via the Internet at http://pubs.acs.org.

AUTHOR INFORMATION

Corresponding Author

* Prof. Svilen Bobev, bobev@udel.edu. Phone: (302)-831-8720. Fax: (302)-831-6335.

Author Contributions

The manuscript was written through contributions of all authors. All authors have given approval to the final version of the manuscript.

Funding Sources

US Department of Energy, Office of Science, Basic Energy Sciences.

ACKNOWLEDGMENT

This work was supported by the U.S. Department of Energy, Office of Science, Basic Energy Sciences, under Award # DE-SC0008885.

REFERENCES

(1) Stoyko, S. S.; Blanchard, P. E. R.; Mar, A. Ternary rare-earth iron arsenides $RE_{12}Fe_{57.5}As_{41}$ (RE = La, Ce). *Inorg. Chem.* **2010**, *49*, 2325–2333.

(2) Xiong, D.-B.; Zhao, Y.; Schnelle, W.; Okamoto, N. L.; Inui, H. Complex alloys containing double-Mackay clusters and $(Sb_{1-\delta}Zn_{\delta})_{24}$ snub cubes filled with highly disordered zinc aggregates: Synthesis, structures, and physical properties of ruthenium zinc antimonides. *Inorg. Chem.* **2010**, *49*, 10788–10797.

(3) He, H.; Tyson, C.; Bobev, S. New compounds with $[As_7]^{3-}$ clusters: Synthesis and crystal structures of the Zintl phases Cs_2NaAs_7, Cs_4ZnAs_{14} and Cs_4CdAs_{14}. *Crystals* **2011**, *1* (3), 87–98.

(4) Suen, N.-T.; Wang, Y.; Bobev, S. Synthesis, crystal structures, and physical properties of the new Zintl phases $A_{21}Zn_4Pn_{18}$ (A = Ca, Eu; Pn =As, Sb)—versatile arrangements of $[ZnPn_4]$ tetrahedra. *J. Solid State Chem.* **2015**, *227*, 204–211.

(5) Lo, C.-W. T.; Ortiz, B. R.; Toberer, E. S.; He, A.; Svitlyk, V.; Chernyshov, D.; Kolodiazhnyi, T.; Lidin, S.; Mozharivskyj, Y. Synthesis, structure, and thermoelectric properties of α-Zn_3Sb_2 and comparison to β-$Zn_{13}Sb_{10}$. *Chem. Mater.* **2017**, *29*, 5249–5258.

(6) Ovchinnikov, A.; Saparov, B.; Xia, S.-Q.; Bobev, S. The ternary alkaline-earth metal manganese bismuthides Sr_2MnBi_2 and $Ba_2Mn_{1-x}Bi_2$ ($x \approx 0.15$). *Inorg. Chem.* **2017**, *56*, 12369–12378.

(7) Brown, S. R.; Kauzlarich, S. M.; Gascoin, F.; Snyder, G. J. $Yb_{14}MnSb_{11}$: New high efficiency thermoelectric material for power generation. *Chem. Mater.* **2006**, *18*, 1873–1877.

(8) Rull-Bravo, M.; Moure, A.; Fernández, J. F.; Martín-González, M. Skutterudites as thermoelectric materials: Revisited. *RSC Adv.* **2015**, *5*, 41653–41667.

(9) Guo, X.; Chen, X.; Altounian, Z.; Ström-Olsen, J. O. Magnetic properties of MnBi prepared by rapid solidification. *Phys. Rev. B* **1992**, *46*, 14578–14582.

(10) Stewart, G. R. Superconductivity in iron compounds. *Rev. Mod. Phys.* **2011**, *83*, 1589–1652.

(11) Gascoin, F.; Sevov, S. C. Niobium-arsenic Zintl phases: A_6NbAs_5 (A = K, Rb, Cs), $K_6NbTlAs_4$, and $K_8NbPbAs_5$ with edge-bridged niobium-centered tetrahedra of arsenic, $[NbAs_4M]^{n-}$ where M = As, Tl, Pb. *Inorg. Chem.* **2002**, *41*, 2820–2825.

(12) Gascoin, F.; Sevov, S. C. Synthesis and characterization of $K_{38}Nb_7As_{24}$ and $Cs_9Nb_2As_6$: The first mixed-valence transition-metal Zintl phases. *Inorg. Chem.* **2002**, *41*, 5920–5924.

(13) Bollore, G.; Ferguson, M. J.; Hushagen, R. W.; Mar, A. New ternary rare-earth transition-metal antimonides RE_3MSb_5 (RE = La, Ce, Pr, Nd, Sm; M = Ti, Zr, Hf, Nb). *Chem. Mater.* **1995**, *7*, 2229–2231.

(14) Bie, H.; Devon Moore, S. H.; Piercey, D. G.; Tkachuk, A. V.; Zelinska, O. Y.; Mar, A. Ternary rare-earth titanium antimonides: Phase equilibria in the RE–Ti–Sb (RE = La, Er) systems and crystal structures of $RE_2Ti_7Sb_{12}$ (RE = La, Ce, Pr, Nd) and $RETi_3(Sn_xSb_{1-x})_4$ (RE = Nd, Sm). *J. Solid State Chem.* **2007**, *180*, 2216–2224.

(15) Bie, H.; Mar, A. Ternary rare-earth titanium antimonides $RE_2Ti_{11-x}Sb_{14+x}$ (RE = Sm, Gd, Tb, Yb). *Inorg. Chem.* **2008**, *47*, 6763–6770.

(16) Bie, H.; Mar, A. $Ba_5Ti_{12}Sb_{19+x}$, a polar intermetallic compound with a stuffed γ-brass structure. *J. Solid State Chem.* **2009**, *182*, 3131–3137.

(17) Adam, A.; Schuster, H.-U. Ternäre intermetallische Phasen des Lithiums mit Elementen der 4. Neben- und 5. Hauptgruppe mit statistischer Metallverteilung im "Kationen"-Teilgitter. *Z. Anorg. Allg. Chem.* **1991**, *597*, 33–39.

(18) Murakami, T.; Yamamoto, T.; Takeiri, F.; Nakano, K.; Kageyama, H. Hypervalent bismuthides La_3MBi_5 (M = Ti, Zr, Hf) and related antimonides: Absence of superconductivity. *Inorg. Chem.* **2017**, *56*, 5041–5045.

(19) Ovchinnikov, A.; Bobev, S. Undistorted linear Bi chains with hypervalent bonding in La_3TiBi_5 from single-crystal X-ray diffraction. *Acta Crystallogr. C* **2018**, *74*, 618–622.

(20) Ovchinnikov, A.; Bobev, S. Synthesis, crystal and electronic structure of the titanium bismuthides $Sr_5Ti_{12}Bi_{19+x}$, $Ba_5Ti_{12}Bi_{19+x}$, and $Sr_{5-\delta}Eu_{\delta}Ti_{12}Bi_{19+x}$ ($x \approx 0.5$–1.0; $\delta \approx 2.4, 4.0$). *Eur. J. Inorg. Chem.* **2018**, *2018*, 1266–1274.

(21) Petříček, V.; Dušek, M.; Palatinus, L. Crystallographic computing system JANA2006: General features. *Z. Kristallogr. Cryst. Mater.* **2014**, *229*, 345–352.

(22) *SAINT; Bruker AXS Inc., Madison, Wisconsin, USA, 2014.*

(23) *SADABS; Bruker AXS Inc., Madison, Wisconsin, USA, 2014.*

(24) Sheldrick, G. M. Crystal structure refinement with *SHELXL*. *Acta Crystallogr. C* **2015**, *71*, 3–8.

(25) Gelato, L. M.; Parthé, E. *STRUCTURE TIDY* – a computer program to standardize crystal structure data. *J. Appl. Crystallogr.* **1987**, *20*, 139–143.

(26) Jepsen, O.; Andersen, O. K. *The Stuttgart TB-LMTO-ASA program, version 4.7; Max-Planck-Institut für Festkörperforschung: Stuttgart, Germany*.

(27) Barth, U. von; Hedin, L. A local exchange-correlation potential for the spin polarized case. I. *J. Phys. C* **1972**, *5*, 1629–1642.

(28) Honda, K. The thermomagnetic properties of the elements. *Ann. Phys.* **1910**, *32*, 1027–1063.

(29) Owen, M. Magnetochemical testings. The thermomagnetic properties of elements II. *Ann. Phys.* **1912**, *37*, 657–699.

(30) Nakamura, A.; Hiranaka, Y.; Hedo, M.; Nakama, T.; Tatetsu, Y.; Maehira, T.; Miura, Y.; Mori, A.; Tsutsumi, H.; Hirose, Y.; Mitamura, K.; Sugiyama, K.; Hagiwara, M.; Honda, F.; Takeuchi, T.; Haga, Y.; Matsubayashi, K.; Uwatoko, Y.; Onuki, Y. Fermi surface and magnetic properties of antiferromagnet $EuBi_3$. *J. Phys. Soc. Jpn.* **2013**, *82*, 124708.

(31) Derrien, G.; Tillard-Charbonnel, M.; Manteghetti, A.; Monconduit, L.; Belin, C. Synthesis and crystal structure of $M_{11}X_{10}$ compounds, M = Sr, Ba and X = Bi, Sb. Electronic requirements and chemical bonding. *J. Solid State Chem.* **2002**, *164*, 169–175.

(32) Kleinke, H. Extraordinarily short Pb–Pb bonds in the new binary intermetallic $Ti_6Pb_{4.8}$. *J. Solid State Chem.* **2001**, *159*, 134–138.

(33) Richter, C. G.; Jeitschko, W. Preparation and crystal structure of the titanium and hafnium bismuthides Ti_8Bi_9 and Hf_8Bi_9. *J. Solid State Chem.* **1997**, *134*, 26–30.

(34) Watanabe, K.; Yamane, H. Crystal Structure of $TiBi_2$. *Acta Crystallogr. E* **2016**, *72*, 1254–1256.

(35) Lütjering, G.; Williams, J. C. *Titanium*; Springer Berlin Heidelberg: Berlin, Heidelberg, 2007.

(36) Pauling, L. *The Nature of the Chemical Bond*; Cornell University Press: Ithaca, NY, 1960.

(37) Tan, W.; Wu, Z.; Zhu, M.; Shen, J.; Zhu, T.; Zhao, X.; Huang, B.; Tao, X.; Xia, S. $A_{14}MgBi_{11}$ (A = Ca, Sr, Eu): Magnesium bismuth based Zintl phases as potential thermoelectric materials. *Inorg. Chem.* **2017**, *56*, 10576–10583.

(38) Hu, Y.; Kauzlarich, S. M. $Yb_{14}MgBi_{11}$: Structure, thermoelectric properties and the effect of the structure on low lattice thermal conductivity. *Dalton Trans* **2017**, *46*, 3996–4003.

(39) Webb, D. J.; Kuromoto, T. Y.; Kauzlarich, S. M. New ternary magnets $(Ca, Sr, Ba)_{14}MnBi_{11}$. *J. Magn. Magn. Mater.* **1991**, *98*, 71–75.

(40) Chan, J. Y.; Wang, M. E.; Rehr, A.; Kauzlarich, S. M.; Webb, D. J. Synthesis, structure, and magnetic properties of the rare-earth Zintl compounds $Eu_{14}MnPn_{11}$ and $Eu_{14}InPn_{11}$ (Pn = Sb, Bi). *Chem. Mater.* **1997**, *9*, 2131–2138.

(41) Chan, J. Y.; Olmstead, M. M.; Kauzlarich, S. M.; Webb, D. J. Structure and ferromagnetism of the rare-earth Zintl compounds: $Yb_{14}MnSb_{11}$ and $Yb_{14}MnBi_{11}$. *Chem. Mater.* **1998**, *10*, 3583–3588.

(42) Ovchinnikov, A.; Prakash, J.; Bobev, S. Crystal chemistry and magnetic properties of the solid solutions $Ca_{14-x}RE_xMnBi_{11}$ (RE = La–Nd, Sm, and Gd–Ho; $x \approx 0.6$–0.8). *Dalton Trans.* **2017**, *46*, 16041–16049.

(43) Papoian, G.; Hoffmann, R. Hypervalent bonding in one, two, and three dimensions: Extending the Zintl-Klemm concept to nonclassical electron-rich networks. *Angew. Chem. Int. Ed.* **2000**, *39*, 2408–2448.

(44) Ferguson, M. J.; Hushagen, R. W.; Mar, A. Crystal structures of La_3ZrSb_5, La_3HfSb_5, and $LaCrSb_3$. Structural relationships in ternary rare-earth antimonides. *J. Alloys Compd.* **1997**, *249*, 191–198.

(45) Tkachuk, A. V.; Muirhead, C. P. T.; Mar, A. Structure and physical properties of ternary uranium transition-metal antimonides U_3MSb_5 (M = Zr, Hf, Nb). *J. Alloys Compd.* **2006**, *418*, 39–44.

(46) Papoian, G.; Hoffmann, R. Building up complexity from strips and sheets: The electronic structure of the $La_{12}Mn_2Sb_{30}$ alloy. *J. Solid State Chem.* **1998**, *139*, 8–21.

(47) Raju, N. P.; Greedan, J. E.; Ferguson, M. J.; Mar, A. $LaCrSb_3$: A new itinerant electron ferromagnet with a layered structure. *Chem. Mater.* **1998**, *10*, 3630–3635.

(48) Ovchinnikov, A.; Makongo, J. P. A.; Bobev, S. Yet again, new compounds found in systems with known binary phase diagrams. Synthesis, crystal and electronic structure of Nd_3Bi_7 and Sm_3Bi_7. *Chem. Commun.* **2018**, *54*, 7089–7092.

(49) Villars, P.; Calvert, L. D. *Pearson's handbook of crystallographic data for intermetallic phases. 2nd ed.*; American Society for Metals: Materials Park, OH, 1991.

(50) Ovchinnikov, A.; Bobev, S. On the effect of Ga and In substitutions in the $Ca_{11}Bi_{10}$ and $Yb_{11}Bi_{10}$ bismuthides crystallizing in the tetragonal $Ho_{11}Ge_{10}$ structure type. *Acta Crystallogr. C* **2018**, *74*, 269–273.

(51) Kohout, M.; Wagner, F. R.; Grin, Y. Electron localization function for transition-metal compounds. *Theor. Chem. Acc.* **2002**, *108*, 150–156.

For Table of Contents Only

A new family of ternary titanium bismuthides, $AE_3Ti_8Bi_{10}$ (AE = Sr, Ba, Eu), has been discovered and characterized. Physical property measurements and first principle calculations indicate metallic behavior and absence of localized magnetism on the Ti atoms. The Ti substructure shows an extensive framework of two-center and multicenter metal–metal interactions.